# 3D Inverse Design of Pumpjet and Study on the Influence of Blade Profile

**Mingyu Zhang[a], Weiqiang Yu, Zhongwei Chen**

China Coast Guard Academy, Ningbo 315801, China

[a]yijianmingyu@163.com

**Keywords:** The rotor blade, the hydraulic performance, structural strength, the pumpjet hydraulic performance

**Abstract:** The rotor blade load decreases successively from shroud to hub with pumpjet operation, so reasonably control of blade area can improve the load distribution of rotor. This paper makes related research on the problem how the change of meridional a ngle between the rotor leading edge and trailing edge influence the hydraulic performance and structural strength. 3 pump jets were designed consists of improved No.19A duct and rotor, stator designed based on 3-D inverse design method, all the blades were thickened based on NACA airfoil. Open water hydraulic characteristics and structural strength of 3 pump jets were calculated and compared after implementing the reliability demonstration of numerical simulation. Results show that, based on the same power, duct and meridional area of rotor blade, an appropriate increase of meridional angle can improve the pumpjet hydraulic performance in safety of intensity.

## 1. Introduction

Pumpjet is mainly composed of a duct, a rotor and a stator [1].The duct can protect the rotor blades, reduce the rotor tip slip loss, insulate waterweeds, prevent the blades from collision damage and the protect the personal safety of drowning, which is similar to duct propeller. The presence of stator can generate a prerotation for the rotor to increase the axial energy component to 99.7%, which exceeds friction loss brought from the stator, the stator is used to fix the duct at the same time. The above mentioned advantages make the safety and efficiency of pumpjet to be higher than that of propeller and duct propeller. In addition, pumpjet has the advantages of low radiation noise and high critical velocity [2]. In recent years, the pumpjet has been gradually applied and developed on submarines (United States Virginia, Seawolf attack submarines and the United Kingdom Trafalgar, Astute attack nuclear submarine, etc.), torpedoes(Mark50, Mark18, etc.), motorboats, amphibious landing vehicles and other fields.

The inverse design method is divided into 2 parts of flow field calculation and blade shape calculation, the blade shape is iteratively improved based on the CFD results of the flow field so as to determine out the optimal impeller only once [3]. Based on this method, Xiao Ruofu made a further optimize of a mixed flow pump to increase the hydraulic efficiency by 3.2% [4]. Yang Wei applied the three-dimensional inverse design method to a centrifugal fan with a self-compiled program and pointed out that the three-dimensional inverse design method could be applied to all kinds of impeller machinery [5]. Jin Shuanbao researched on the effect of blade heavy load position of a axial flow pump to cavitations and hydraulic efficiency based on three-dimensional inverse design method and CFD numerical simulation[6], the design efficiency of a mixed flow pump is as high as 90.5%[7]. Chang Shuping researched on the influence of circulation distribution on rotor blade trailing edge to a mixed flow pump based on three-dimensional inverse design method [8]. But studies on the hydraulic performance influenced by blade profile are relatively shallow. This study combined with three dimensional inverse design and CFD numerical simulation to research on the influence of blade profile (controlled by a gradual rise of the meridian angle between rotor blade leading edge and trailing edge) to hydraulic characteristic based on the same power and blade area. Three pump jets were designed out and their structural strength was analyzed together.

## 2. Three-dimensional inverse problem design theory

The flow is assumed as inviscid and incompressible and the blade is assumed as infinitely thin. Effect of the blade on flow is instead by vortex sheet, whose principle of blade design is consistent with the arc method. Vortex intensity is expressed as circumferential circulation $2\pi r\bar{V}_\theta$ [9-10]. The velocity field is decomposed into the circumferential mean velocity and periodic velocity in solving the 3-D positive proposition in cylindrical coordinates:

$$\vec{V} = \bar{\vec{V}} + \tilde{\vec{V}} \tag{1}$$

Assuming that inflow is uniform, incompressible, inviscid and irrotational. $\nabla \cdot \bar{V} = 0$ and $\tilde{\vec{V}} \cdot \vec{n} = 0$, we get the mean flow equation in blade area:

$$\frac{\partial^2 \Psi}{\partial r^2} - \frac{1}{r}\frac{\partial \Psi}{\partial r} + \frac{\partial^2 \Psi}{\partial z^2} = -r[\frac{\partial f}{\partial z}\frac{\partial r\bar{V}_\theta}{\partial r} - \frac{\partial f}{\partial r}\frac{\partial r\bar{V}_\theta}{\partial z}] \tag{2}$$

And the mean flow equation in non-blade area:

$$\frac{\partial^2 \Psi}{\partial r^2} - \frac{1}{r}\frac{\partial \Psi}{\partial r} + \frac{\partial^2 \Psi}{\partial z^2} = 0 \tag{3}$$

Where $\vec{n}$ is surface normal vector, $\Psi$ is a introduced stream function, $f$ is the blade wrapping angle, $r\bar{V}_\theta$ is mean velocity moment. $\tilde{\vec{v}}$ is incompressible, continuous and its curl equals to periodic component of helicity, so the periodic flow equation in blade area can be obtained combined with Clebsh formula.

$$\nabla^2 \Phi(r,\theta,z) = T(S) \cdot \nabla^2 r\bar{V}_\theta + T'(S)(\nabla r\bar{V}_\theta \cdot \nabla S) \tag{4}$$

And the periodic flow equation in non-blade area is

$$\nabla^2 \Phi(r,\theta,z) = 0 \tag{5}$$

Where $T(S) = \sum_{K=1}^{\infty} \frac{2}{KB}\cos(KBf)\sin(KB\theta) - \sum_{K=1}^{\infty} \frac{2}{KB}\sin(KBf)\cos(KB\theta)$, $\Phi$ is the potential function, $S$ is the blade position function, $B$ is the number of blades.

Inverse proposition is to be solved based on that no-slip velocity boundary condition is satisfied on blade surface, the relative velocity vector always tangents to blade surface and is thus perpendicular to blade surface normal vector. So the equation of the blade shape is obtained as follow:

$$(\bar{V}_Z + v_{zb1})\frac{\partial f}{\partial z} + (\bar{V}_r + v_{rb1})\frac{\partial f}{\partial r} = \frac{r\bar{V}_\theta}{r^2} + \frac{v_{\theta b1}}{r} - \omega \tag{6}$$

Where $\omega$ is the rotation speed, solution and iteration of forward and inverse proposition can finally determine out the optimal rotor or stator. The relative velocity of the upper and lower blade surface is perpendicular to both the blade surface normal vector and direction of curl, then the relative velocity can be switched to:

$$W_b^+ - W_b^- = \frac{2\pi}{B}\frac{\left(\nabla r\bar{V}_\theta \times \nabla S\right)\times \nabla S}{\nabla S \times \nabla S} \tag{7}$$

For incompressible flow the pressure loading on the blade is directly related to the meridional derivative of $r\bar{V}_\theta$ (blade loading), namely

$$P^+ - P^- = \frac{2\pi}{B}\rho W_{mbl}\cdot\frac{\partial r\bar{V}_\theta}{\partial m} \tag{8}$$

Here $P^+$ is the upper blade surface pressure, $P^-$ is the lower blade surface pressure and $W_{mbl}$ is the relative meridional blade surface velocity, $m$ is the meridional blade streamline length, the value of $r\bar{V}_\theta$ is equal to the integration of $\partial r\bar{V}_\theta / \partial m$ along $m$. Thus distribution of $\partial r\bar{V}_\theta / \partial m$ is important to pump performance, this loading method of $\partial r\bar{V}_\theta / \partial m$ can control the design result more effectively [11-12]. Finally, the three-dimensional viscous flow field of the pumpjet is calculated by the software CFX to obtain the accurate hydraulic characteristics.

## 3. Pumpjet design parameters and geometric solution

Three pump jets are designed using the same duct which is improved from the 19a duct. Inlet diameter is 0.213m, nozzle diameter is 0.268m, rotation Speed is 2200r/min, the inflow speed is 42km/h and the power rating is 35kw. The number of rotor blades is defined as 4 and its tip clearance is 0.25mm. The number of stator guide vanes is defined as 6, the three pump jets were recorded as No. 1, No. 2 and No.3, whose meridional geometries are shown in Fig.1.

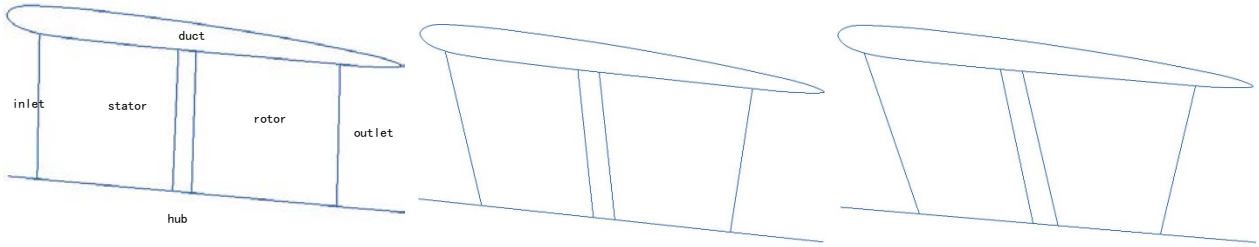


No. 1 pumpjet No. 2 pumpjet No. 3 pumpjet

Figure 1. Meridional geometry for the three pump jets

Here the included angle between rotor leading edge and rotor trailing edge of No. 1 pumpjet is 0°, the included angles of No. 2 pumpjet and No. 3 pumpjet are 15°and 30°respectively, the distance between the rotor and stator and the rotor meridional area of three pump jets are the same. All blades are thickened based on NACA airfoil and the maximal thickness is 4 mm. rotors and the stators obtained from the three-dimensional inverse design matching on the duct improved from 19a duct can finally determine out the three pumpjets showed as Fig.2.

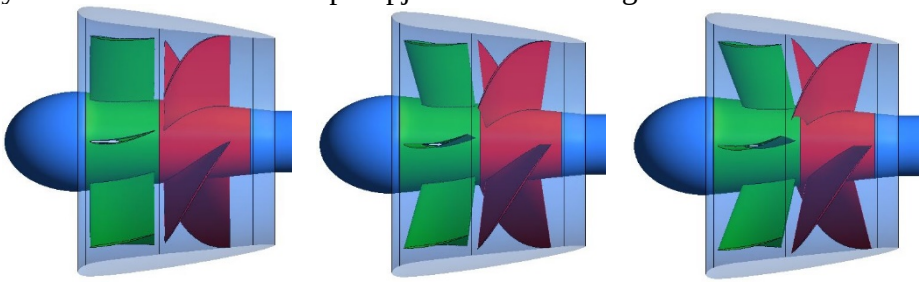

No. 1 pumpjet No. 2 pumpjet No. 3 pumpjet

Figure 2. 3-D shape for the pumpjet

The $r\bar{V}_\theta$ can be nondimensionalized after being divided by reference value $R_{ref}U_{ref}$, where $R_{ref}=\sqrt{R_{Hub}^2+R_{Shr}^2}$ and $U_{ref}=2\pi R_{ref}n/60$. Taking No.3 pumpjet as an example, dimensionless load distribution of rotor and stator blades are shown in Fig.3 and Fig.4, then the load distribution of the whole blade can be obtained by linear interpolation. Where $m$ is the relative position of the corresponding blade from the leading edge to the trailing edge, "0" represents the leading edge and"1" represents the trailing edge. The load distribution is parabolic in both ends and the middle section is nearly a horizontal line [12].

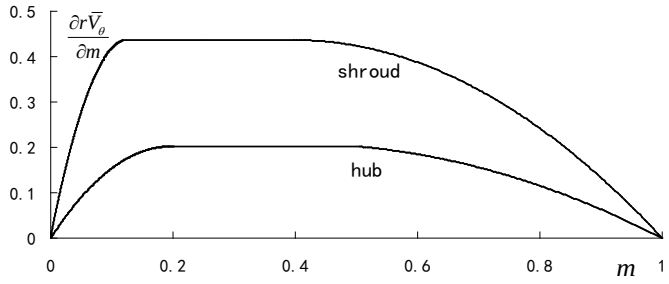


Figure 3. Rotor blade loading on and shroud

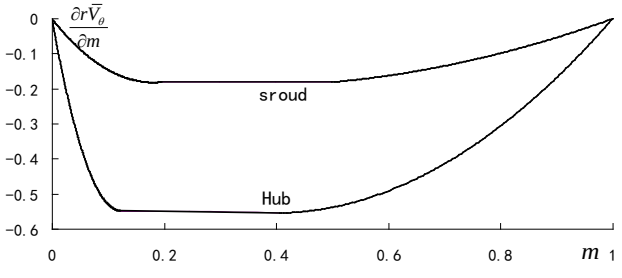


Figure 4. Stator blade loading on hub and shroud

## 4. Calculation of open water characteristics of pump jets

The RANS equation is solved by using the SST turbulence model based on the software CFX. The SST turbulence model calls $k-\varepsilon$ turbulence model and SST turbulence model in free flow region and near wall region respectively through a mixing function, which integrates the advantages of the two turbulence model to simulate the viscous sublayer better [13].

In order to verify the credibility of the numerical simulation method, calculation and verification of open water characteristics of E779A propeller is worked out in this paper. The propeller diameter is 0.227m, the pitch is 0.25m, there are 4 blades and the disk area ratio is 68.9%. The calculation domain settings and structured grids are shown in Fig.5, where D is the propeller diameter.

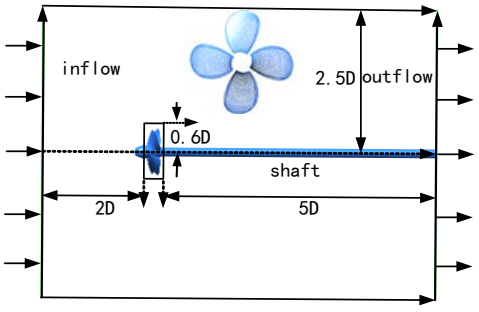


Figure 5. Computational domain and boundary conditions

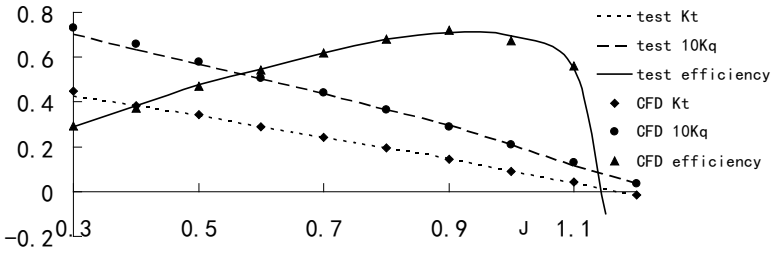


Figure 6. Results comparison with experimental data

According to test conditions of related document [14], we defined the rotation speed n=707.3rpm, advance coefficient J=0.3-1.2 .the thrust coefficient $K_t$, torque coefficient $K_q$ and propeller efficiency $\eta$ under different advance coefficient could be obtained through the software CFX. Where $K_t=T/\left(\rho n^2D^4\right)$, $K_q=Q/\left(\rho n^2D^5\right)$ and $\eta=JK_t/\left(2\pi K_q\right)$. Fig.6 shows that the thrust coefficient and torque coefficient are in good agreement with the experimental results in a large range, the maximum relative error is 3.1% between the calculated value and the experimental data, which verified the credibility of the numerical calculation. More numerical validation information can consult relevant papers the author has published such as document [15] and [16].

Calculation of pump jets using full structured grids showed as Fig.7, whose calculation domain settings is completely consistent with that of the propeller. To No.1 pumpjet, for example, the

streamline of 42km/h is shown in Fig.8. Cavitations phenomenon doesn't occur in Stator vanes and rotor blades pressure surface of three pump jets. The pressure distribution on the suction surface of the rotor blade is shown in Fig.9, where the blue area are the cavitations zone. The internal flow of the rotor is complex and the extent of the previous exhibition of rotor blades becomes larger with the increase of the included angle, which makes the secondary flow to be the most serious in the vicinity of the rotor inlet near the hub under the influence of the interaction of rotor and stator, and local cavitations begin to generate here in No.3 pumpjet. The axial energy component Ec of the outlet jet is defined as:

$$\iint_S V_z^2 / \left(V_\theta^2 + V_r^2 + V_z^2\right) \tag{9}$$

Where $V_z$, $V_r$, $V_\theta$ is the axial, radial and circumferential velocity of pumpjet outlet respectively and S is the outlet area.

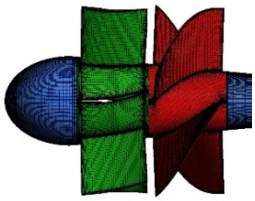

Figure 7. Structural mesh of pumpjet

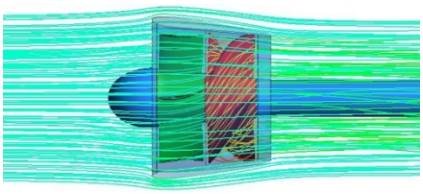

Figure 8. Streamlines of open water pumpjet

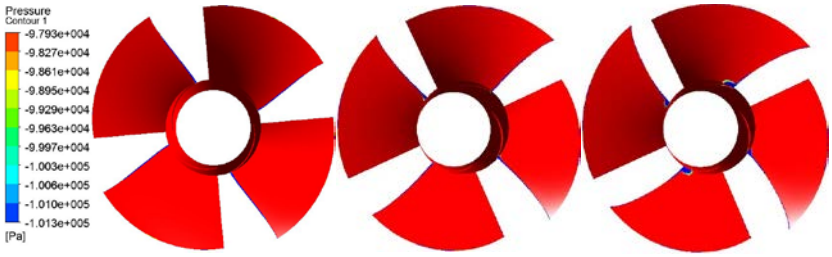


Figure 9. Pressure distribution on the suction surface of the rotor blades

The calculation of 5 working conditions of the three pump jets is carried out in this study based on the rotation speed of 2200r/min and the inlet velocity ranging from 39-48km/h. The hydraulic characteristic parameters are shown in TABLE 1:

Table 1. CFD results of 3 pump jets

| $V$ (km/h) | | 39 | 42 | 43.5 | 45 | 48 |
|---|---|---|---|---|---|---|
| $Q$(kg/s) | No.1 | 523.02 | 535.01 | 539.04 | 544.00 | 555.03 |
| | No.2 | 523.04 | 535.03 | 539.06 | 544.03 | 555.06 |
| | No.3 | 523.02 | 535.01 | 539.03 | 544.01 | 555.02 |
| $H$(m) | No.1 | 8.12 | 7.42 | 7.27 | 7.05 | 6.54 |
| | No.2 | 8.18 | 7.52 | 7.39 | 7.17 | 6.64 |
| | No.3 | 8.14 | 7.46 | 7.32 | 7.10 | 6.60 |
| $P$(kW) | No.1 | 46.61 | 43.44 | 42.76 | 42.04 | 40.20 |
| | No.2 | 46.63 | 43.48 | 42.81 | 42.10 | 40.29 |
| | No.3 | 46.57 | 43.46 | 42.82 | 42.13 | 40.38 |
| $E_c$(%) | 99.19 | 99.30 | 99.34 | 99.38 | 99.43 | 99.19 |
| | 99.00 | 99.13 | 99.21 | 99.26 | 99.30 | 99.00 |
| | 98.89 | 99.02 | 99.10 | 99.15 | 99.18 | 98.89 |
| $\eta$(%) | No.1 | 89.3 | 89.6 | 89.9 | 89.5 | 88.6 |
| | No.2 | 90.0 | 90.7 | 91.1 | 90.8 | 89.7 |
| | No.3 | 89.6 | 90.1 | 90.4 | 89.9 | 88.9 |

Under the similar power, the axial energy component of outlet jet keeps decreasing with the increase of the included angle between rotor leading edge and rotor trailing edge. The head and efficiency of pump jets at first increases and then decreases and is the highest for the No.2 pump jet.

## 5. Calculation and analysis of the rotor strength

Finite element modeling and mesh generation is carried out for the rotor blades and the mesh is identified as 129600 elements finally, which can meet the requirements of the calculation accuracy. The Model and grids are shown in Fig.10.

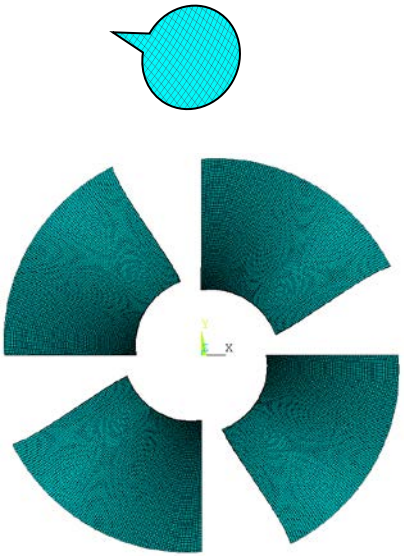

Figure 10. Finite element model and mesh of impeller

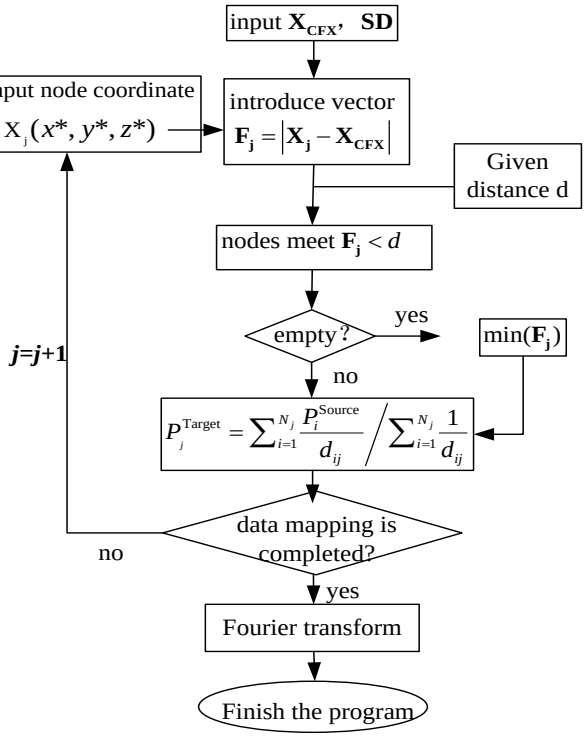


Figure 11. Flow chart of data projection

The material of the rotor is duplex stainless steel whose main material properties are shown in TABLE 2:

Table 2. Rotor material properties pump jets

| Material | Yield limit $\sigma_s$/Mpa | Strength limit $\sigma_b$ /Mpa | Young modulus E/Gpa | Poisson ratio u | Density $\rho$/(kg/m$^3$) |
|---|---|---|---|---|---|
| Duplex Stainless Steel | 550 | 750 | 210 | 0.33 | 7850 |

The blade root is fixed in the finite element calculation of the rotor strength. Gravity loads are applied by means of the gravity acceleration and centrifugal loads are applied by means of the rotation angular velocity. The hydrodynamic loads are mapped from blades in computed flow fields in the design point (2200r/min, 42km/h) of 3 pump jets. The data mapping Method from flow field grids to the finite element meshes are shown in Fig.11.

Stress nephograms of three rotors under above loads are as follows:

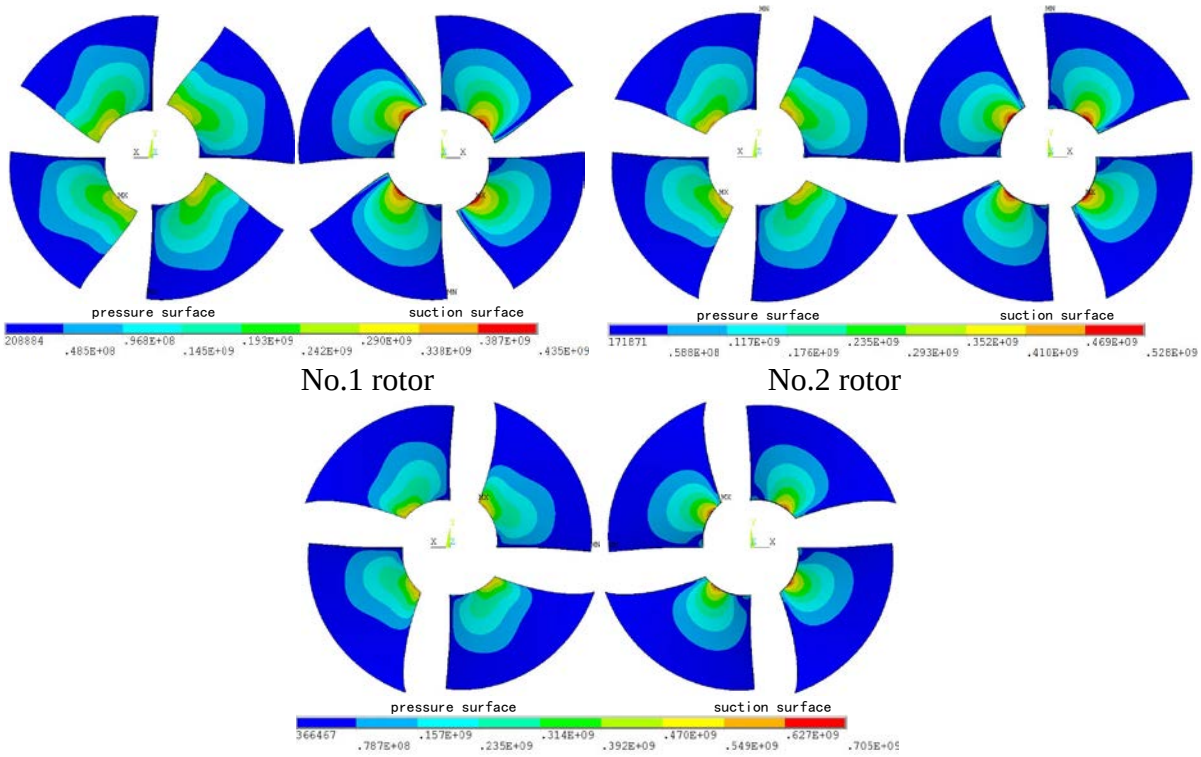


Figure 12. Stress nephograms of blades suction surface under combined loads

The results show that the maximum stress of the rotor is concentrated at the blade root near the leading edge, the maximum stress of 3 rotors is 435Mpa, 528Mpa, 705Mpa respectively with the increase of the included angle between the leading edge and the trailing edge. Yield limit and Strength limit of duplex stainless steel is 550Mpa and 750Mpa respectively, so the No.3 pumpjet doesn't meet the strength requirements.

## 6. Conclusion

It is fast and efficient to design the rotor and stator based on 3-D inverse design method. The blade load distribution can be effectively controlled by the control of velocity moment. The NACA thickness distribution of blades and the improved No.19A duct are used to solve the problems of pumpjet duct design and thickening of blades.

1) Taking propeller E779A as the object to validate the reliability of numerical calculation, based on which the hydraulic characteristics of three pump jets are calculated and analyzed. Results show that the head and efficiency of pump jets increases firstly and then decreases with the increase of the angle between rotor leading edge and rotor trailing edge, which reaches the highest value for the No.2 pumpjet, and serious secondary flow leads to cavitations in the vicinity of the rotor inlet near the hub in the No.3 pumpjet.

2) The maximum stress of the rotor is concentrated at the blade root near the leading edge based on the results of strength calculation and the maximum value increases with the increase of the included angle, No.3 pumpjet doesn't meet the strength requirements of duplex stainless steel.

3) In summary, there is an optimal value of the included angle between rotor leading edge and rotor trailing edge which can meet the needs of strength and cavitations and improve the head and efficiency of pumpjet at the same time. So the results were available in theory analysis and engineering application.

**Acknowledgments**

This work was financially supported by key disciplines program (Military Equipment) in Ningbo and Fund Project: National Nature Science Foundation of China (51309229);

Zhang Mingyu (1989), Male, doctor, Email addresses: yijianmingyu@163.com.

**References**

[1] Pan Guang, Hu Bin, Wang Peng, et al. Numerical Simulation of steady hydrodynamic performance of a pumpjet propulsor [J].Journal of Shang Hai Jiao Tong University, 2013, 47 (6): 992 - 937.

[2] Wang Tiankui, Tang Denghai. Pumpjet Propulsor-Low Noise Propulsor of Nuclear Submarine [J]. Conmilit, 2006 (7): 52 - 54.

[3] Bonaiuti D, Zangeneh M. On the coupling of inverse design and optimization techniques for the multiobjective, multipoint design of turbomachinery blades [J]. Journal of Turbomachinery, 2009, 131: 021014.

[4] Xiao Ruofu, Tao Ran, Wang Weiwei. 3-D inverse design and hydrodynamic performance optimization for a mixed-flow pump impeller [J]. Transactions of the Chinese Society for Agricultural Machinery, 2014, 45 (9): 84 - 88.

[5] Yang Wei, Wang Fujun, Wang Hong. Three-dimensional inverse design and fluid flow numerical simulation for centrifugal impeller [J]. Journal of Drainage and Irrigation Machinery Engineering, 2012, 30 (4): 632 - 635.

[6] Jin Shuanbao, Wang Yongsheng. 3-D design of axial-flow pump and numerical prediction of its cavitation performance [J]. Journal of Drainage and Irrigation Machinery Engineering, 2013, 31(9): 763 - 767.

[7] Jin Shuanbao, Wang Yongsheng, Ding Jiangming, et al. Three-dimensional design and numerical experiment of mixed-flow waterjet with CFD [J]. Journal of Harbin Engineering University, 2012, 33 (10): 1223 - 1227.

[8] Chang Shuping, Shi Yanfeng, Zhou Chen, et al. Effects of Exit Circulation Distribution on Performances of Mixed-flow Pump [J]. Transactions of the Chinese Society for Agricultural Machinery, 2014, 45 (1): 89 - 93.

[9] Luo Xingqi. Three dimensional inverse problem calculation and all three dimensional inverse problem calculation of the Francis Turbine Runner [D]. Beijing: Department of hydraulic engineering, Tsinghua University, 1995.

[10] Guan Xingfan. Handbook of modern pump technology [M]. Beijing: Astronavigation Press, 1995.

[11] Goto A, Nohmi M, Sakurai T, et al. Hydrodynamic design system for pumps based on 3-D CAD, CFD and inverse design method [J]. ASME Journal of Fluids Engineering, 2002, 124 (2): 329 - 335.

[12] Bonaiuti D, Zangeneh M, AartojarviR, et al. Parametric design of a waterjet pump by means of inverse design, CFD calculations and experimental analyses [J]. ASME Journal of Fluids Engineering, 2010, 132: 1 - 15.

[13] Lloyd G, Espanoles A. Best practice guidelines for marine applications of computational fluid dynamics[R]. WS Atkins Consultants and Members of the NSC, MARNET-CFD Thernatic Network, 2002.

[14] PumpLinx Demonstration on Performance and Cavitation of E779A Propeller. Geometry and Experimental Data Courtesy of INSEAN, 2009, 09. Http: //www.insean.it.

[15] Zhang Mingyu, Lin Ruilin, WangYongsheng, et al, Numerical prediction and analysis of underwater radiated noise of no-shaft Pumpjet [J]. Journal of Ship Mechanics, 2018, 22 (11): 1323 - 1332.

[16] Zhang Mingyu, Lin Ruilin, WangYongsheng, et al. The 3-D Inverse Design of A Pumpjet and Its Opening Water Performance Comparison with the origin propeller [J]. Journal of Harbin Engineering University, 2017, 38 (5): 690 - 696.